VIII International Conference on Fracture Mechanics of Concrete and Concrete Structures
FraMCoS-8
J.G.M. Van Mier, G. Ruiz, C. Andrade, R.C. Yu and X.X. Zhang (Eds)

A novel experimental method to characterize the cyclic response of the crack tip process zone in a quasi-brittle material

Erwan Morice, Sylvie Pommier

LMT-Cachan, 61 avenue du Président Wilson, 94235 Cachan, France
email : name@lmt.ens-cachan.fr

Key words: Quasi-brittle, Multi-scale, Toughness Measurement, Subcritical Crack Growth

Abstract: A novel experimental method was developed to measure the cyclic response of the process zone at crack tip in a mortar. The test geometry was designed so as to measure both the fracture toughness and the fatigue crack growth rate using the same specimen and hence the same material. The tests conducted showed that a subcritical crack growth by fatigue occurs in this material. The displacement field around the crack tip was measured during fatigue cycling using digital images correlation and later post-treated so as to extract the non-linear cyclic response of the process zone. To do so the measured mode I velocity field was partitioned into two parts, the first one characterizing the linear elastic response of the cracked structure while the second one carries the non-linear behavior of the process zone. Each part is also approximated as the product of a weighting function and of an intensity factor. The intensity factor that characterizes the non-linear response of the process zone was determined during fatigue cycling.

1. INTRODUCTION

Quasi-brittle materials, such as concrete or mortar, show a non-linear behavior in cyclic tension which stems, amongst other factors, from the nucleation, the growth and the coalescence of micro cracks [1-5].

The initial elastic properties of the material (step 1) deteriorate because of the nucleation of micro-cracks (step 2) up to a critical point for which strain and damage localization occurs (step 3).

The drop of the material elastic properties due to micro-cracking can be determined at the onset of an unloading step (step 4).

After unloading, some permanent strains remain and partial stiffness recovery is observed (step 5) which can be explained, amongst other phenomena, by the micro-crack closure and friction.

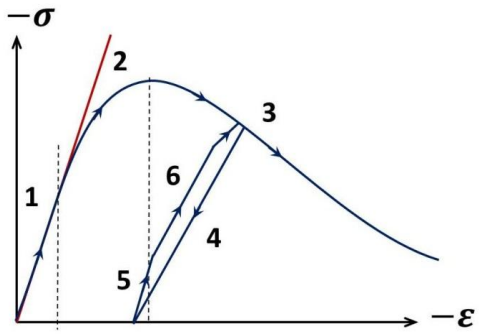

Figure 1. Schematics of the behavior of a quasi-brittle material.

Within the process zone at crack tip, the same set of phenomena also occurs. Various approaches [6-8] have hence been developed to derive the fracture properties of a quasi-brittle material from the continuum damage constitutive behavior (Fig. 1).

To do so a non-local approach is mandatory. As matter of fact, viewing the stress and the strain as local becomes highly questionable once the strain localization has occurred, i.e. beyond the step 2 in Fig. 1. And it is precisely the behavior of the material

determined once the strain localization has occurred that is the most relevant for fracture problem, since ahead of a crack tip, the strain field is "geometrically" localized by nature.

This study is therefore focused on the experimental characterization of the non-linear response of the process zone at crack tip using a non-local approach. Various non-local approaches are proposed in the literature. In [8] for instance, the authors assume that the damage distribution is explicitly defined as a function of the distance to a level set. In this paper a similar analysis is done, except for the weighting function that is not given arbitrarily but determined directly from experiments.

This experimental method derives from a technique that was used to analyze crack tip plasticity in metals [9-11] either using experimental velocity fields measured by DIC [9] or using finite element results [10,11] in mode I or in mixed mode conditions.

This technique is based on the following considerations.

First, the process zone is assumed to be fully constrained by a linear elastic bulk. This constraint limits drastically the actual number of degrees of freedom required to characterize the response of the crack tip process zone.

Second, to some extent, the geometry of a crack is self-similar with respect to the crack tip and therefore the velocity field is expected also be self-similar, that is to say, is expected to be the product of an intensity factor (degree of freedom) and a self-similar spatial distribution.

Third, by merely reversing the loading direction, it is always possible to get, at least transiently, a linear elastic behavior of the material within the process zone. This implies that the linear and the non-linear responses are two independent phenomena that can be characterized independently and that are characterized independently by an intensity factor (degree of freedom) and a self-similar spatial distribution.

Finally, the displacement field in each time step dt within the local coordinate system attached to the crack plane and front in a quasi-brittle material is assumed to be the superposition of:

- the displacement field relative to the linear elastic response of the process zone, considering its current state of damage, characterized by the intensity factor $d\tilde{K}_I$. This term being the sum of the contribution of the nominal stress intensity factor dK_I^∞ and of the shielding effect of the process zone onto the macro crack, characterized by $\left(d\tilde{K}_I - dK_I^\infty\right)$.
- the displacement field related to the non-linear behavior of the process zone, characterized by the intensity factor $d\rho_I$,

The velocity field in the vicinity of the crack tip is hence approximated by Eq.1:

$$\underline{v}(P,t) = \dot{\tilde{K}}_I(t)\underline{u}^e(P) + \dot{\rho}_I(t)\underline{u}^{pz}(P) \quad (1)$$

In Eq. (1), $\underline{u}^e(P)$ and $\underline{u}^{pz}(P)$ are two reference fields relative to the linear elastic behavior of the macro-crack and that of the process zone, that describe the spatial distribution of each part around the crack front and that are used as weighting functions to approximate the velocity field at crack tip.

The main objective of these experiments was to determine these two weighting functions $\underline{u}^e(P)$ and $\underline{u}^{pz}(P)$ and the evolution of damage and hence of ρ_I during fatigue cycling as a function of the nominal stress intensity factor K_I^∞.

To do so, a special specimen was used in order to get a stable crack growth during monotonic and cyclic loading. The velocity fields and the crack lengths were measured using the digital image correlation program Q4-DIC [12,13].

2. MATERIAL AND EXPERIMENTS

a. Test specimen

To perform the experiments a prismatic beam was tested in axial compression (Fig. 2). The beam has a through thickness cylindrical hole in its center that induces a tensile stress concentration at the two poles of the hole during compression. The traction stress

decreases with the distance from the hole before vanishing.

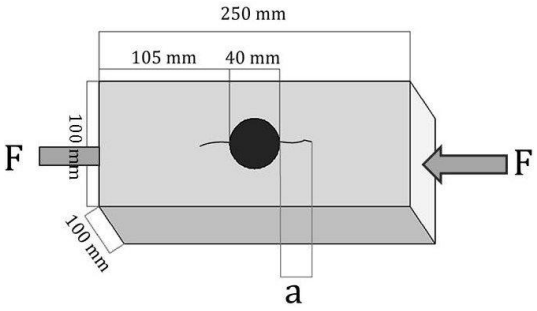

Figure 2. Specimen geometry

The nominal stress intensity factor evolution for a coplanar double crack initiated at the two poles of the cylinder (Fig. 2) was determined using linear elastic finite element analyzes (Fig. 3).

The stress intensity factor decreases with the crack extent ***a*** from each pole, over a distance between ***a*** = 2 mm and ***a*** = 50 mm. Beyond **a** =50 mm the slope of the curve changes and the stress intensity factor increases (Fig. 3). The crack growth is stable between ***a*** = 2 mm and ***a*** = 50 mm.

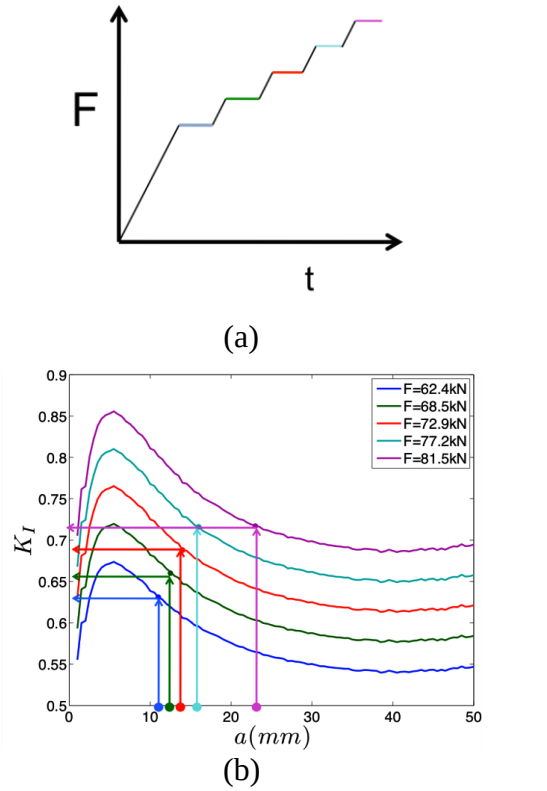

Figure 3.: (a) Loading sequence applied to perform repeated measurements of K_{Ic}.
(b) determination of K_{Ic} using the measurement of the arrested crack length.

b.Fracture toughness

The decay of the nominal stress intensity factor with the crack length is very useful because for a given compression load F**,** the crack is arrested when the crack length is such as that the nominal stress intensity factor K_I^∞ is just below the fracture toughness K_{Ic}. The arrested crack length is determined using digital image correlation [12,13]. The evolution of $K_I^\infty(a)$ determined from linear elastic finite element analyses, allows determining K_{Ic} using the arrested crack length a (Fig. 3).

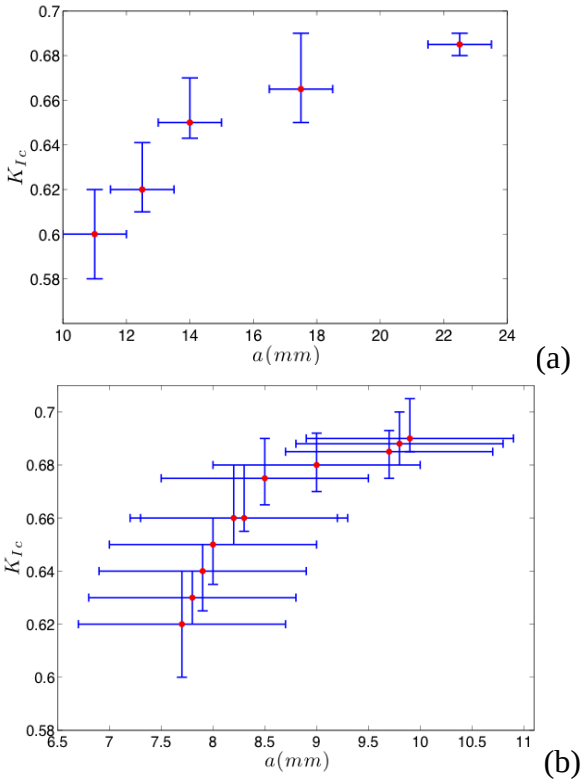

Figure 4.: Evolution of the measured fracture toughness with the crack extent in monotonic compression, the error bars indicate the uncertainty associated with the measurement of the crack extent and that associated with the fracture toughness. (a) first specimen, (b) second specimen.

This geometry allows also performing repeated measurement of the fracture toughness using the same specimen. In addition, the slope dK_I^∞/da is small enough so that the quite large uncertainty associated with the measurement of the arrested crack length a would correspond to a very small uncertainty on K_{Ic} (Fig. 3). It is worth to

underline that the uncertainty associated with the measurement of the arrested crack length a in Fig. 4 is an upper bound. The uncertainty has been overestimated so as to guarantee the result of the measurement of K_{Ic} in all cases.

In Fig. 4b, it is observed that the fracture toughness increases with the crack length over a distance of 2 to 8 mm before stabilizing at $K_{Ic} \approx 0.69MPa\sqrt{m}$ in both tests. In the first test (Fig. 4 a) the load applied on the specimen was higher (Fmax=90kN) than in the second specimen (Fmax=70kN) (Fig. 4 b).

The observed increase of the fracture toughness is believed to be associated with the development of a damaged wake along the crack faces that produces a shielding effect onto the macro-crack. The crack extent required to measure a stabilized value of K_{Ic} should be well above the diameter of the damaged zone associated with crack initiation so that the measured value of K_{Ic} would be characteristic of crack propagation and not of crack initiation (Fig. 5).

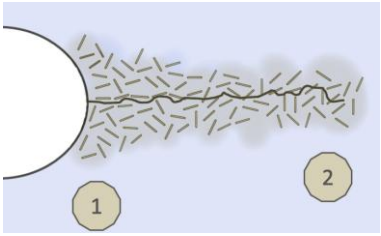

Figure 5.: Illustration of the development of a damages wake. (1) damaged zone associated with crack initiation, (2) process zone and damaged wake for a crack growing at $K_I = K_{Ic}$

c. Creep test

The objective of these experiments is primarily to analyze fatigue crack growth. However during fatigue cycling a subcritical crack growth by creep may also occur. In order to discriminate the individual contributions of creep and of fatigue, a creep test was also performed before performing the fatigue test.

Using the same protocol as for toughness measurements, the specimen was loaded in compression and the arrested crack length was determined at the end of the loading ramp (F_{max}). The value of the fracture toughness value was measured at:

$$K_{Ic} \approx 0.69MPa\sqrt{m}$$

The compression load F_{max} was then maintained and the arrested crack length was determined after a period of 36 hours of creep without any detectable crack propagation, i.e. the crack growth rate is below 10^{-6} mm.h^{-1}. The threshold for creep crack growth could hence be determined and is equal to:

$$K_{Ith}^{creep} \approx 0.66MPa\sqrt{m}$$

After this point, the specimen was then subjected to fatigue cycles with a maximum compression load F_{max}=70 kN and a load ratio R=0.1 in order to measure fatigue crack growth by fatigue below the threshold for creep crack growth.

d. Subcritical crack growth by fatigue

In this test, a subcritical crack growth by fatigue was clearly observed but the fatigue threshold could not be determined because two crack branches were visible on the surface of the specimen and grew simultaneously. The distance between the two crack tips being small, less than 10 mm, the two tips are interacting and the stress intensity factor determination was questionable.

A third experiment was therefore conducted to observe fatigue crack growth.

The specimen was first loaded monotonically and the fracture toughness was determined so as to get a stabilized value of the fracture toughness before the beginning of the fatigue test (Fig. 4b). The maximum load applied to determine K_{Ic} is F_{max}=70 kN. Once the fracture toughness has reached its saturation value, the specimen was then subjected to fatigue cycling with F_{max}=70 kN, a load ratio R=0.5 and at 5 Hz. The loading scheme is plotted in Fig. 6 (a) and the measured crack growth rate in Fig. 6 (b).

The crack length was measured periodically during the test so as to determine the crack growth rate (Fig. 6 b). By applying a linear fit on the crack propagation by cycle curve, we measured a mean subcritical crack growth rate of 4.3 nm per cycle.

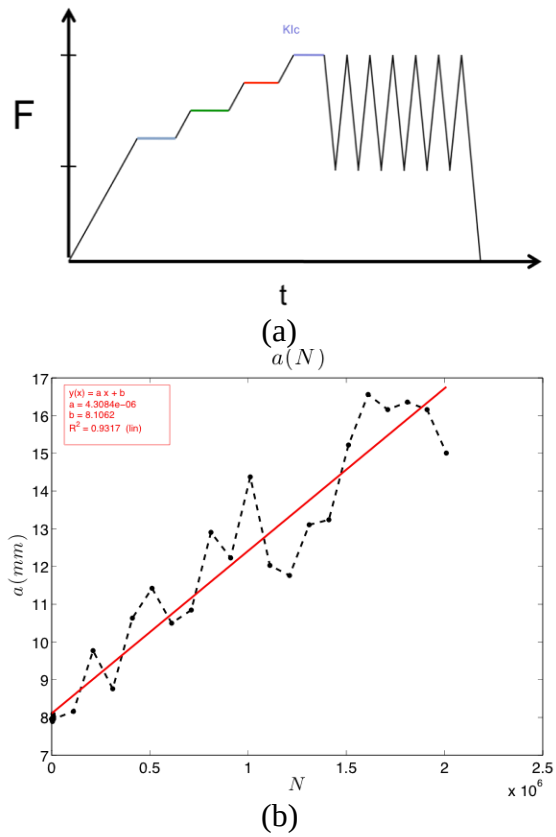

Figure 6.: Loading scheme (a) and measured crack propagation (b) during fatigue cycling at 5Hz and R=0.5.

The arrested crack length was also determined after a period of 48 hours of fatigue cycling at 5 Hz without any detectable crack growth using the DIC analysis which yields a fatigue threshold for this mortar equal to:

$$\Delta K_{Ith}^{fatigue} \approx 0.3\ MPa\sqrt{m} \text{ at R=0.5}$$

The measured fatigue threshold is well below both the fracture toughness and the threshold for creep crack growth.

3. NON-LOCAL CYCLIC RESPONSE OF THE PROCESS ZONE

At this point, the crack remained arrested during fatigue cycling with F_{max}=70 kN and F_{min}=35 kN. The next step of the experiment was then to determine the non-linear response of the crack tip process zone during cycling.

Since damage, stresses and strains are localized in this problem a non-local approach is used to post-treat the experimental results. This non local approach is tailored for this problem.

a. Assumptions

In these analyses, the mode I behaviour only is analyzed. Additional analyzes were done in mixed mode conditions that are not reported here, but it is worth to mention that the same methodology can be applied in mixed mode I+II conditions [9,14].

First of all, the nominal stress intensity factor K_I^∞ is determined in the LEFM framework, using the compression load applied on the test specimen and the crack length determined using DIC.

Then the specimen is loaded cyclically and the load signal is used to trigger the capture of images so as to get 22 images per cycle.

The crack tip is first located and the images are then cropped to position the tip of the crack in the center of the image and the crack plane midway. This operation is equivalent to removing the rigid body motion from the total displacement field.

Then the displacement field relative to the frame attached to the crack plane and tip is extracted from the sequence of images [12,13]. Then, it is partitioned into mode I and mode II components (Eq. 2, 3, 4) using symmetry considerations.

$$\underline{v}(P,t) = v_I(x,y,t) + v_{II}(x,y,t) \tag{2}$$

$$\begin{cases} 2v_{Ix} = v_x(x,y,t) + v_x(x,-y,t) \\ 2v_{Iy} = v_y(x,y,t) - v_y(x,-y,t) \end{cases} \tag{3}$$

$$\begin{cases} 2v_{IIx} = v_x(x,y,t) - v_x(x,-y,t) \\ 2v_{IIy} = v_y(x,y,t) + v_y(x,-y,t) \end{cases} \tag{4}$$

It is checked that the mode II part of the displacement field is negligible with respect to the mode I part.

Then, the mode I part is partitioned into two terms (Eq. 1). The first one characterizes the displacement field of the macro-crack (considering the effect of the nominal loads and the shielding effect of the process zone) and the second one characterizes the non-linear behavior of the process zone. To do so, it was first necessary to construct the two reference fields $\underline{u}^e(P)$ and $\underline{u}^{pz}(P)$ that are used to approximate the displacement field using Eq. (1).

b. Construction of the reference fields

To identify the elastic reference fields, three cycles were applied with the load amplitude corresponding to the fatigue threshold, i.e. with F_{max}=70 kN and F_{min}=35 kN.

For each cycle, eleven images were captured during the loading phase and during the unloading phase. The images were post-treated using digital image correlation [12,13] to determine the displacement field $d\underline{u}(P,dt)^{DIC}$ associated with each couple of images.

The crack being arrested, the behavior of the process zone is believed to behave essentially elastically. In such a case, for each time step dt, the approximation in Eq. (1) reduces to :

$$d\underline{u}(P,dt)^{DIC} = dK_I^{\infty}(dt)\underline{u}^e(P) \qquad (5)$$

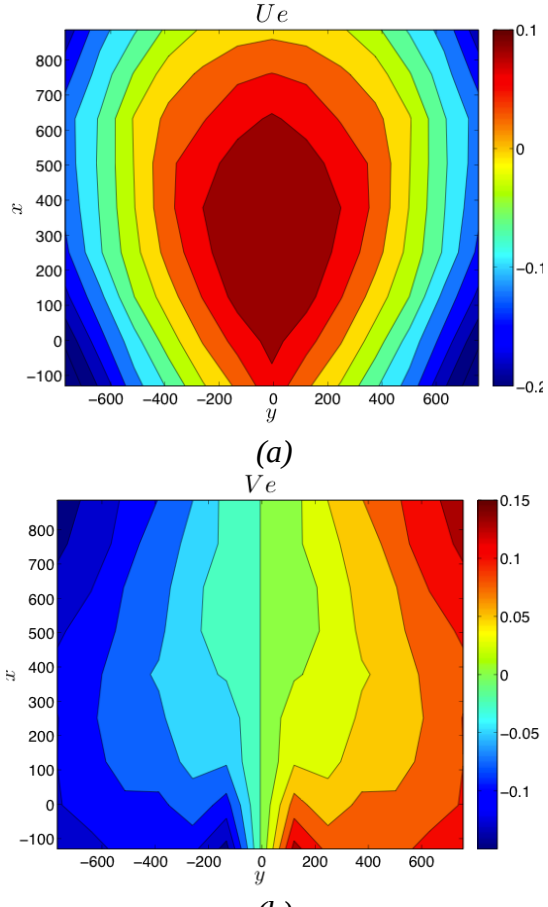

Figure 7.: Experimental elastic reference field in mode I. (a) intensity of the component parallel to the crack plane, (b) intensity of the component normal to the crack plane.

The nominal stress intensity factor variation dK_I^{∞} between two images is calculated using the load increment dF_{max} applied on the specimen and the arrested crack length. This allows determining $\underline{u}^e(P)$ for each couple of images using Eq. (5). Finally, to limit the measurement errors and the noise on the elastic field, the elastic reference field $\underline{u}^e(P)$ is calculated as the average of the fields determined for each loading or unloading ramp and for the three fatigue cycles.

The two components of the elastic reference field are plotted in Fig.7.

The intensity of the component V_e normal to the crack plane is discontinuous across the crack faces and symmetric.

Once the elastic reference field is identified, the specimen was then fatigued above the fatigue threshold so as to get a non-linear response of the process zone.

The specimen was subjected to a cyclically increasing loading amplitude keeping the mean value constant (Fig. 8 a).

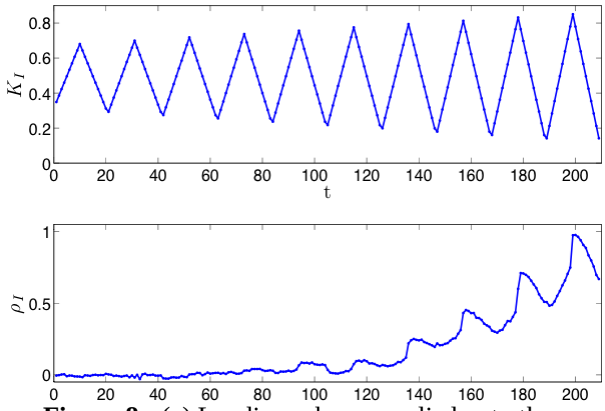

Figure 8.: (a) Loading scheme applied onto the specimen and (b) evolution of the intensity factor $\rho_I(t)$ that characterizes the non-linear response of the process zone.

For each loading and unloading ramp, 10 images are captured and the displacement field between two images is determined by DIC. The displacement field is partitioned into mode I and mode II components considering the crack tip position identified during the fatigue cycles at the fatigue threshold. The mode I component is then

projected onto the mode I elastic reference field $\underline{u}^e(P)$ as follows:

$$d\widetilde{K}_I(t) = \frac{\sum_{P\epsilon D} d\underline{u}(P,dt)^{DIC}.\underline{u}^e(P)}{\sum_{P\epsilon D} \underline{u}^e(P).\underline{u}^e(P)} \quad (6)$$

The residue of this projection (Eq. 7) is then determined for each time step:

$$d\underline{u}(P,t)^{residue} = d\underline{u}(P,t)^{DIC} - d\widetilde{K}_I(t)\underline{u}^e(P) \quad (7)$$

In order to construct the reference field $\underline{u}^{pz}(P)$ that characterizes the behavior of the process zone, we used a Karhunen-Loeve transform.

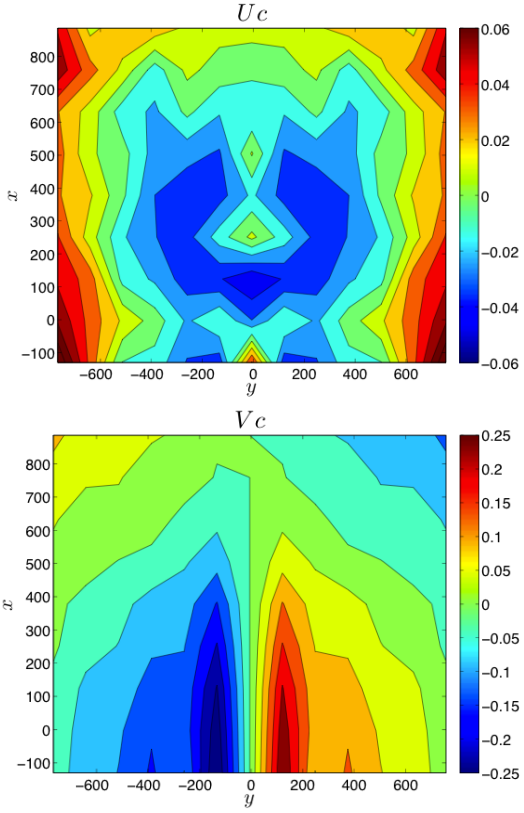

Figure 9.: Experimental complementary reference field in mode I

The Karhunen-Loeve transform is a proper orthogonal decomposition, that allows to enlighten independent or uncorrelated displacements. Applied on a spatial-temporal matrix, where for each column is assigned the displacement field at the time *t*, and for each line the value of $d\underline{u}(P,t)^{residue}$ in a given point *P* through time, the spatial self-correlation matrix of the displacement field is built. The eigenvector associated to the highest eigen-value of this matrix correspond to the reference field $\underline{u}^{pz}(P)$ ignoring a multiplying factor. The two components of the reference field $\underline{u}^{pz}(P)$ are plotted in Fig. 9.

The intensity of the *V* components of the complementary field is highly localized in the vicinity of the crack tip and decreases with the distance to the crack tip. This result is consistent with the fact that the process zone is well constrained inside an undamaged bulk.

Once the reference field $\underline{u}^{pz}(P)$ is constructed, the intensity factor variation $d\rho_I$ in each time step is determined as follows:

$$d\rho_I(t) = \frac{\sum_{P\epsilon D} d\underline{u}(P,dt)^{DIC}.\underline{u}^{pz}(P)}{\sum_{P\epsilon D} \underline{u}^{pz}(P).\underline{u}^{pz}(P)} \quad (8)$$

The evolution of $\rho_I(t)$ during cycling is plotted in Fig. 8 (b). During the first cycles, for which the amplitude corresponds to the fatigue threshold, the value of $\rho_I(t)$ remains negligible. Then, it is observed that the mean value and the amplitude of $\rho_I(t)$ increase with the loading amplitude.

The error $C_{2R}(t)$ associated with the approximation in Eq. (1) of the measured field $d\underline{u}(P,t)^{DIC}$ was also determined as follows:

$$C_{2R}(t) = \frac{\sqrt{\sum_{P\epsilon D}\left(d\underline{u}(P,t)^{DIC} - d\widetilde{K}_I(t)\underline{u}^e(P) - d\rho_I(t)\underline{u}^{pz}(P)\right)^2}}{\sqrt{\sum_{P\epsilon D}\left(d\underline{u}(P,t)\right)^2}} \quad (9)$$

The error $C_{1R}(t)$ associated with a linear elastic approximation of $d\underline{u}(P,t)^{DIC}$ is also calculated as follows:

$$C_{1R}(t) = \frac{\sqrt{\sum_{P\epsilon D}\left(d\underline{u}(P,t)^{DIC} - d\widetilde{K}_I(t)\underline{u}^e(P)\right)^2}}{\sqrt{\sum_{P\epsilon D}\left(d\underline{u}(P,t)\right)^2}} \quad (10)$$

The evolution of the two errors measured during the experiments is plotted in Fig. 10. It is observed that these error remain small (below 10%), and that in certain loading step the error $C_{1R}(t)$ associated with an elastic approximation of $d\underline{u}(P,t)^{DIC}$ is well above that associated with a non-linear approximation

$C_{2R}(t)$ indicating the presence of damage during these time steps.

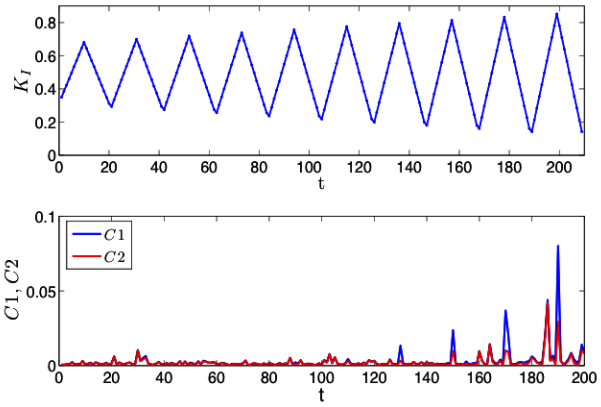

Figure 10.: Evolution of C_{1R} and C_{2R} during cyclic loading.

c. Results - non-linear response of the process zone at crack tip

This analyzes makes it possible to plot the non-linear response of the process zone at crack tip. The nominal stress intensity factor K_I^∞ applied during fatigue cycling was plotted against the intensity factor ρ_I that characterizes the non-linear behavior of the process zone in Fig. 11.

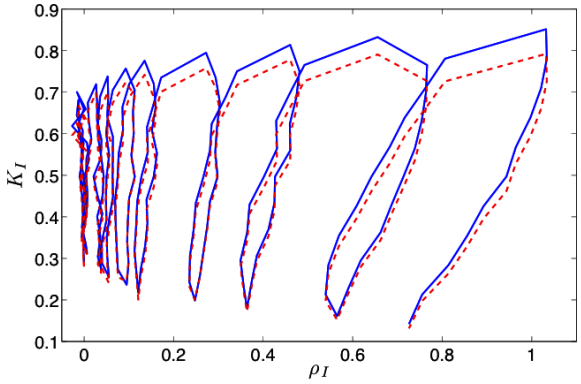

Figure 11.: Evolution of experimental intensity factors. The solid line corresponds to the lower bound for the crack length and the dashed line to the upper bound.

Since the crack grows during fatigue cycling, the entire analyze was repeated for two possible crack length, the first one corresponding to a lower bound for the crack length (before fatigue cycling and considering the lower bound for the uncertainty) and the second one to an upper bound (after cycling, and considering the upper bound for the uncertainty). The curve is not significantly modified according to the assumption regarding the location of the crack tip.

The evolution is very similar to that of an uncracked quasi-brittle material. At first, the curve is vertical, then the slope decreases when the degree of damage increases. A permanent displacement is also observed, that is believed to stem from friction between the micro-cracks faces.

It is important to underline that the reference field $\underline{u}^{pz}(P)$ determined in these experiments (Fig. 9b) has a component normal to the crack plane that is discontinuous across the crack faces. Since the part of the displacement field associated with the process zone in Eq. (1) is approximated by $d\rho_I(t)\underline{u}^{pz}(P)$ the discontinuity is directly proportional to $d\rho_I(t)$. In other words $d\rho_I(t)$ measures also the evolution of the crack tip opening displacement during fatigue cycling (CTOD).

The results plotted in Fig. 11 indicate that the CTOD increases significantly during fatigue cycling.

It is also observed in Fig. 11 that the maximum stress intensity factor K_I^∞ applied during fatigue cycling is well above the fracture toughness. This result was carefully checked. Fatigue cycling may allow a higher density of micro-cracks to be nucleated inside the process zone which may increase the shielding effect onto the macro-crack and hence explain this apparent increase of the resistance to fracture of the material.

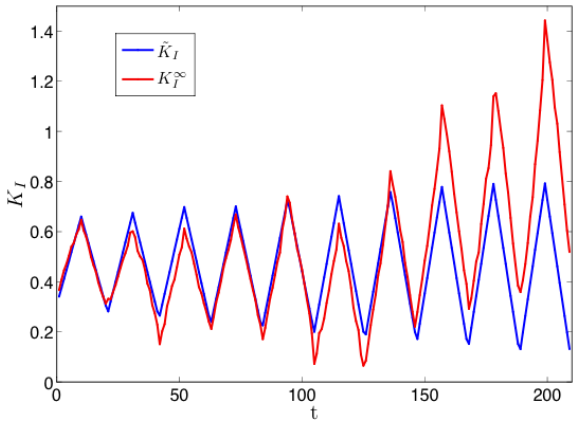

Figure 12.: Evolution versus time of the nominal applied stress intensity factor K_I^∞ and of the intensity factor of the reference elastic field $\underline{u}^e(P)$ determined using the displacement field at crack tip $\tilde{K}_I$

The intensity factor $\widetilde{K}_I$ of the reference elastic field $\underline{u}^e(P)$ is plotted in Fig. 12. As a matter of fact, this term includes the effects of both the remote stresses and the internal stresses (shielding effect of micro-cracks). It is obvious in this graph that the apparent stress intensity factor $\widetilde{K}_I$ determined using the displacement field is very different from that determined using the applied loads K_I^∞ as soon as the degree of damage around the crack tip is significant, indicating a large shielding effect.

4.CONCLUSIONS

A novel experimental approach was proposed to analyze the non-linear response of a cracked quasi-brittle material. Because of the localized nature of the mechanical fields at crack tip, a non-local approach is used.

However, instead of using arbitrary weighting functions for this non-local approach, we used reference fields determined directly from the experiments. The response of the crack tip region is hence represented as the product of an intensity factor (the degree of freedom) and a reference field (the weighting function). In addition, the response is partitioned into two terms, one characterizing the elastic response of the macro-crack, including the shielding effect of the micro-cracks, and the other ρ_I characterizing the non-linear response of the process zone. In addition, ρ_I could also be viewed as the CTOD.

The degree of freedom ρ_I associated with the non-linear response of the process zone was plotted against the nominal applied stress intensity factor. The response of the process zone is analogous to the tensile cyclic stress-strain curve of a quasi-brittle material, showing a progressive degradation of the material properties and an increase of the CTOD with fatigue cycling.

The test specimen used for these experiments allowed also determining the fracture toughness of the material, the threshold for creep crack growth and the fatigue threshold at R=0.5 and 5 Hz.

REFERENCES

[1] Mazars J, Berthaud Y, Ramtani S. The unilateral behavior of damage concrete. *Engng Fract Mech* 1990(35):629–35.

[2] Chaboche JL, Lesne PM, Maire JF. Phenomenological damage mechanics of brittle materials with description of the unilateral damage effect. In: Bazant ZP et al., editors. Fracture and damage in quasibrittle structures. London: E.& F.N. Spon Pubs.; 1994. p. 75–84.

[3] Willamand K, Warnke E. Constitutive model for triaxial behaviour of concrete. In: Proc. concrete and structures subjected to triaxial stresses. Zurich: *Int. Ass. for Bridge and Structural Engineering*; 1975. p. 1–30.

[4] Ortiz M. A constitutive theory for the inelastic behavior of concrete. *Mech. Mater.* 1985(4):67–93.

[5] Desmorat R., Chambart M., Gatuingt F., Guilbaud D., Delay-active damage versus non-local enhancement for anisotropic damage dynamics computations with alternated loading, *Engineering Fracture Mechanics* 77 (2010) 2294–2315

[6] Mazars J., Pijaudier-Cabot G., From damage to fracture mechanics and conversely : A combined approach, *Inf. J. Solids Structures* Vol. 33, No. Z&22, pp. 3327-3342, 1996.

[7] Comi C., Mariani S., Perego U., An extended FE strategy for transition from continuum damage to mode I cohesive crack propagation, *Int. J. Numer. Anal.* Methods Geomech. 31 (2007) 213–238.

[8] Bernard P.E., Moës N., Chevaugeon N., Damage growth modeling using the Thick Level Set (TLS) approach: Efficient discretization for quasi-static loadings, *Comput. Methods Appl. Mech. Engrg*. 233–236 (2012) 11–27

[9] Decreuse P.Y., Pommier S., Poncelet M., and Raka B., A novel approach to model mixed mode plasticity at crack tip and crack growth. Experimental validations using velocity fields from digital image correlation. *International Journal of Fatigue*, 42 :271 – 283, 2012.

[10] Pommier S., Lopez-Crespo P., Decruse P.Y., A multi-scale approach to condense the cyclic elastic-plastic behaviour of the crack tip region into an extended constitutive model. *Fatigue & Fracture of Engineering Materials & Structures*. Vol 32. Pages 899-915. 2009

[11] Fremy F., Pommier S., Galenne E., and Courtin S.. A scaling approach to model history effects in fatigue crack growth under mixed mode I+II+III loading conditions for a 316l stainless steel. *International Journal of Fatigue*, 42 :207 – 216, 2012.

[12] Mathieu F., Hild F. and Roux S., Identification of a crack propagation law by digital image correlation. *International Journal of Fatigue*, 36(1) :146 – 154, 2012.

[13] Besnard G., Hild F. and Roux S., "Finite-element" displacement fields analysis from digital images: Application to Portevin–Le châtelier bands. *Experimental Mechanics*, 46:789–803,2006

[14] Morice E., Pommier S., Delaplace A. Non-linear fracture mechanics, a novel approach for quasi-brittle materials. First IJFatigue & FFEMS Joint Workshop - Characterisation of Crack Tip Stress Fields. 2011. .